

CHARACTERIZING LOCAL CONTACT RESISTANCES OF INTERDIGITATED BACK CONTACT SILICON SOLAR CELLS

Milan Padilla¹, Bernhard Michl¹, Christian Reichel¹, Nikolaus Hagedorn¹, Sven Kluska¹, Stephen T. Haag¹, Roman Keding¹, Andreas Fell², Martin Kasemann², Wilhelm Warta¹, Martin C. Schubert¹

¹Fraunhofer Institute for Solar Energy Systems ISE, Heidenhofstr. 2, D-79110 Freiburg, Germany

²College for Engineering and Computer Science, Australian National University, Canberra, ACT, 2602 Australia

³Department for Microsystems Engineering, University of Freiburg, D-79110 Freiburg, Germany

*Corresponding author - Phone: +49 (0) 761 4588 5263 Fax: + 49 (0) 4588 9250

Email: milan.padilla@ise.fraunhofer.de

ABSTRACT: Next generation high efficiency interdigitated back contact (IBC) silicon solar cells are often designed with complex doping and contacting structures that are sensitive to series resistance induced losses. Particularly local contact resistance problems present a major fill factor loss in industrially feasible solar cell designs. In this work, we use advanced two dimensional device simulations to understand the impact of globally and locally deteriorated electron and hole contacts on a typical IBC design. For a set of examples, the effect of an increased contact resistance on the global current voltage characteristic is compared to the signature of a simulated local series resistance image using luminescence imaging. Consistent interpretations and quantitative agreement between global and local analysis are shown. We find that the local series resistance of IBC cells react identically for globally altered electron and hole contact resistances. However, locally deteriorated electron and hole contact resistances do not impact fill factor losses identically. Together with qualitative interpretation of luminescence images, these findings present valuable information for IBC cell manufacturers for understanding their cell design's sensitivity to local contact resistance or broken finger problems on fill factor and short-circuit current.

Keywords: silicon, solar cells, IBC, series resistance, contact resistance, luminescence

1 INTRODUCTION

The pursuit for increasingly more efficient yet industrially feasible silicon solar cells has led to cell designs with selective doping areas (e.g. selective emitters, local back-surface-fields (BSF)), point contacts and other advanced structures such as interdigitated back contact (IBC) silicon solar cells [1, 2]. Optimizing such solar cell concepts towards more economical, industrial processes, e.g. larger structures and alternative metallization techniques, is related to the challenge of increased series resistance (R_S) caused by prolonged current paths or poor local contact resistances. Spatially resolved analysis is crucial to distinguish between local and global (homogeneous) power losses [3]. IBC silicon solar cells, which have all contacts and the metallization on the rear side, are a promising high efficiency concept for mass fabrication. The recent 25.6 % world record efficiency was reached by Sanyo/Panasonic on an IBC structure [4] and SunPower Corp. as a pioneer on IBC cells has achieved 25.0% and industrially fabricates IBC cells with over 24% efficiency [5]. Furthermore, numerous companies are developing competitive and industrial feasible IBC cell designs. However, only little on spatially resolved characterization of these complex cells has been published.

When it comes to series resistance problems in IBC cell fabrication, one may distinguish between limitations to the fill factor (FF) by design (pitch distance, cell thickness, base doping, sheet resistances, grid metallization) and by unintended local problems. For the later, broken fingers, poor or inexistent local contacts are the common phenomena. These defects often occur locally.

In this work, we study local and global contact resistance problems on a line contacted IBC cell structure and discuss how local problems affect the IV characteristics. We find that there is a dependency on

which of the electron or hole contacts is affected and how this is observable and quantifiable through luminescence series resistance imaging.

Unlike regular cells, where current flows mainly vertically along the base, there are major lateral current flows of electrons and holes in IBC cells. These currents flow opposite to each other through the base and in the emitter (EM) and back surface field (BSF) or front surface field (FSF) regions where they present majority carriers. A schematic of this current flow is shown in Figure 1.

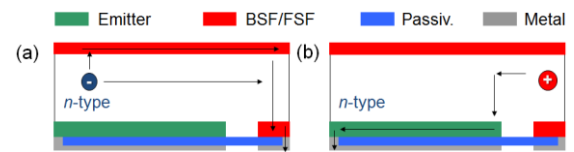


Figure 1: Schematic cross section with current flows of a typical n-type IBC cell for electrons (a) and holes (b)

When performing conventional spatially resolved series resistance (R_S^{loc}) imaging, e.g. according to Trupke et al. [6], the periodic doping structure of IBC cells creates a periodic R_S^{loc} profile for cells. This is a result of interplay between series resistance for electrons and holes and effects of their lateral transport. A discussion on such an asymmetric current transport effect in IBC cells may be found elsewhere [7].

In this work, we define series resistance (R_S) as a power loss mechanism according to the one-diode model for solar cells. R_S at maximum power point (MPP) conditions is then linked to a reduction in global FF in the illuminated current-voltage (IV) curve while not affecting the pseudo fill factor (pFF) of a current-free suns- V_{OC} measurement [8]. This power loss can be caused both by transport losses in the form of joule heat and by recombination which can also be referred to as diffusion resistance [9]. We define R_S^{loc} in a terminal-

connected diode model as the resistance from an image pixel to the terminal. The basic equation is

$$V_{loc-imp} = V_{bias} - R_s^{loc} \cdot J_{loc} ; J_{loc} < 0 \text{ at MPP.} \quad (1)$$

$V_{loc-imp}$ is the local implied voltage at the solar cell rear side, i.e. the contact side of the device. This presents conceptual difference to standard, both-side contacted, cells with full emitter coverage on the front side. A discussion on the validity of this approach can be found elsewhere [7]. V_{bias} is the bias voltage applied at the terminal and J_{loc} the local effectively extracted current density. The lumped R_s of a solar cell can be described as a combination of multiple resistances such as sheet- (R_{SH}), contact- (R_C), bulk- and finger resistance, depending on the specific current paths [10]. Each charge carrier type experiences a different set of resistance contributions through its current path of lowest total resistance. The net current flows of electrons and holes are however never independent because the total current between electrons and holes must balance.

2 IV CHARACTERISTICS OF GLOBALLY AND LOCALLY INCREASED CONTACT RESISTANCES

In the next step, two-dimensional device simulations using the solar cell simulator Quokka [11] are performed to understand the impact of globally and locally poor contact resistances on the total IV performance. Quokka has been validated to be in excellent agreement with Sentaurus simulations on similar IBC devices [12]. A schematic of the unit cell that was used for the following simulations is depicted in Figure 2.



Figure 2: Schematic of the IBC unit cell used to describe locally poor or broken emitter (EM) or BSF contacts. The arrows point at the locations of the targeted manipulations

The relevant parameters for the following simulations of an n-type IBC unit-cell are $\rho_{base} = 1 \Omega\text{cm}$, $J_0^{EM} = 100 \text{ fA/cm}^2$, $J_0^{BSF} = 100 \text{ fA/cm}^2$, $J_0^{FSF} = 15 \text{ fA/cm}^2$, $J_0^{GAP} = 1 \text{ fA/cm}^2$, $R_{sh}^{EM} = 50 \Omega\text{cm}^2$, $R_{sh}^{BSF} = 50 \Omega\text{cm}^2$, $R_{sh}^{FSF} = 400 \Omega\text{cm}^2$. The n-type IBC solar cell has a $1 \Omega\text{cm}$ base resistivity and is $180 \mu\text{m}$ thick, each emitter diffusion is $950 \mu\text{m}$, and each BSF diffusion is $300 \mu\text{m}$ wide with $20 \mu\text{m}$ wide contact openings each. R_C on all contacts of the reference IBC cell was set to $1 \text{ m}\Omega\text{cm}^2$ ("good" contact), which lead to simulated IV parameters as shown in Table I. Since IBC cells even of $1 \Omega\text{cm}$ base resistivity operate in medium or even at high injection conditions, a dogmatic distinction between majority and minority carriers in the base is not suitable.

Table I shows simulated IV parameter results that reveal the cell performance deterioration compared to the reference when a specific emitter or BSF contact is made "poor" ($R_C = 10 \text{ m}\Omega\text{cm}^2$) or "broken" ($R_C = 1000 \text{ m}\Omega\text{cm}^2$). We define a "broken" contact as a contact with very high R_C that allows close to or no current conduction at all under any operating conditions.

The two dimensional model assumes that the contact resistance over the entire finger is extremely high. In a three-dimensional device, there needs to be a distinction between a totally interrupted metal finger and locally extremely high contact resistance (e.g. passivation failed to open for contacting). The latter affects carrier extraction locally at J_{SC} while a destroyed finger also affects the cell far away from the break point. V_{OC} (684 mV) and pFF (84.0 %) results are not further listed for each scenario, because leaving all J_0 values constant leads to an unchanged V_{OC} and pFF .

When using the same geometrical contact area and homogeneously increasing R_C of the emitter (EM) (p^+) or the BSF (n^+) compared to the reference it has the same effect on the IV characteristics in form of a FF loss, see globally "poor" contacts in Tab. I. This identical behavior can be described by an additional resistance that linearly contributes to the global R_s in a diode model.

Table I : IV and R_s simulation results for different scenarios of local and global contact resistance problems.

	J_{SC} (mA/cm ²)	FF (%)	Eta (%)	R_s global (Ωcm^2)	R_s^{loc} mean (Ωcm^2)
Reference $R_C = 1 \text{ m}\Omega\text{cm}^2$					
Reference	39.3	80.1	21.5	0.74	0.74
Globally "poor" contacts $R_C = 10 \text{ m}\Omega\text{cm}^2$					
Globally poor EM	39.3	75.0	20.1	1.72	1.72
Globally poor BSF	39.3	75.0	20.1	1.72	1.72
1 x Locally "poor" contact $R_C = 10 \text{ m}\Omega\text{cm}^2$					
1x poor EM	39.3	78.8	21.1	0.93	1.07
1x poor BSF	39.3	79.4	21.3	0.85	0.87
1 x Locally "broken" contact $R_C = 1000 \text{ m}\Omega\text{cm}^2$					
1x broken EM	35.1	79.2	19.0	0.89	0.85
1x broken BSF	39.3	78.8	21.0	1.00	1.13

The situation becomes more complex when studying the effect of a locally poor or even "broken" contact. As depicted in Fig. 2, one EM or BSF contact out of five in the unit cell is targeted. In the case of the locally poor contact ($R_C = 10 \text{ m}\Omega\text{cm}^2$), no effect on J_{SC} is observed for either EM or BSF contact, but FF is lowered. Here, the poor EM contact has a larger effect on FF than the BSF contact. This asymmetry is caused by the very different current paths and R_{SH} the carrier types need to travel through to reach their respective electron or hole contacts, as shown in the schematic in Fig. 1. More specifically, the poor EM contact acts as an effectively increased resistance for hole conduction through that unit cell. Part of the excess holes will then travel towards the next available EM finger. Some of these carriers will certainly recombine on that way which could be described as resistance limited enhanced recombination [13]. For the electrons, poor current conduction in the BSF can be compensated by transport in the cell via the base or FSF to the next BSF finger. Whether the FF

deterioration is more sensitive to a poor EM or BSF contact depends on the specific combination of geometry (pitch distance), base conductivity and individual R_{SH} in the device.

For the case of a locally "broken" contact ($R_C = 1000 \text{ m}\Omega\text{cm}^2$), we observe a much more pronounced impact on the IV parameters for the EM contact than for the BSF contact. Now, an extreme increase of the EM contact resistance strongly reduces the global J_{SC} , since only few minority carriers (holes) from around the broken EM can be collected at all. We note that the FF also drops, due to the increased distance for holes through the base. On the other hand, if we simulate a broken BSF contact, we obtain no drop of J_{SC} but only a loss in FF . Therefore, according to the definition of R_S in this work (impact on FF in IV characteristic), the broken EM contact yields a smaller contribution to R_S than the poor EM contact. Of course the overall performance due to J_{SC} drop is much lower for the broken EM contact case. Tab. I also includes a simulated R_S global from an IV analysis using the conventional double-light method [14].

3 SERIES RESISTANCE IMAGE CHARACTERISTIC OF GLOBALLY AND LOCALLY INCREASED CONTACT RESISTANCES

In order to study the effects observed on the IV characteristics in the previous section, we chose to perform series resistance imaging using the conventional R_S^{loc} imaging approach first presented by Trupke et al. [6]. It follows the equation

$$R_S^{loc} = \frac{V_{bias} - V_{loc-imp}}{J_{sc}^{loc} - J_0 \exp(V_{loc}/V_T)} \quad (2)$$

J_0 is the global saturation current density (assumed to have no spatial distribution) and J_{SC}^{loc} is the local short-circuit current density. In the conventional R_S^{loc} imaging methods, J_{SC} is assumed to be constant [15, 16]. However, in IBC cells this is often not a good approximation due to the effect of insufficient diffusion lengths ("electrical shading") [17]. A spatially resolved J_{SC}^{loc} however presents a correction but does not fundamentally change the results, as will be discussed in a further investigation.

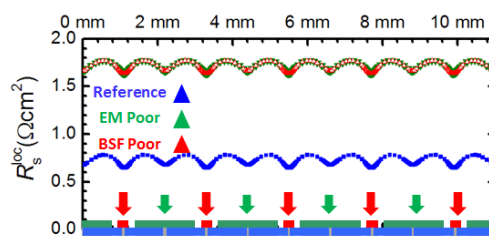
Fig. 3 depicts simulated profiles of R_S^{loc} images for the cases of globally poor EM or BSF contacts (a), a single "poor" EM or BSF contact (b) and a "broken" EM or BSF contact (c). The doping schematic at the bottom of the images serves as a guide to the eye. The cell modelling parameters were the same as for the IBC cells shown in Tab. I. The IV results were obtained from a simulation of all required luminescence images needed in the experiments. This was based on an advanced luminescence model presented in [18]. To obtain the simulated R_S^{loc} images, all usually required experimental images (low illumination V_{OC} , J_{SC} for calibration, J_{SC} at 1 sun and MPP at 1 sun) were simulated in Quokka using the luminescence detection model presented in [18]. More details on how the R_S^{loc} simulations were performed can be found elsewhere [7].

Globally poor EM or BSF contacts (see Tab. I) had an identical response in the IV characteristic. Now, also

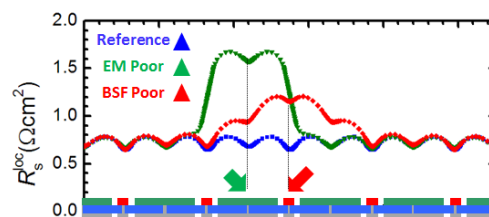
the R_S^{loc} profile is completely independent of which of the two carrier selective contact types is deteriorated. The entire profile was shifted by an offset of $1.0 \text{ }\Omega\text{cm}^2$. We interpret that when one carrier type is globally hindered from flowing through the solar cell, the other current is reduced by the same amount since the net electron and hole current must cancel out. Therefore, the R_S^{loc} images do not yield information on which contact limits the R_S . This implies that the lateral variations of R_S^{loc} in a homogeneous sample are only governed by lateral charge carrier flow [7].

For the case of a locally poor contact (b), we observe that R_S^{loc} significantly increases over the individually targeted contacts. The poor EM shows a greater average R_S^{loc} than the poor BSF, which is consistent with the study of global R_S in the previous section where the FF was more sensitive to the emitter's local R_C^{EM} than the BSF one.

a) Globally „poor“ contacts $R_C = 10 \text{ m}\Omega\text{cm}^2$



b) 1x Locally „poor“ contact $R_C = 10 \text{ m}\Omega\text{cm}^2$



c) 1x Locally „broken“ contact $R_C = 1000 \text{ m}\Omega\text{cm}^2$

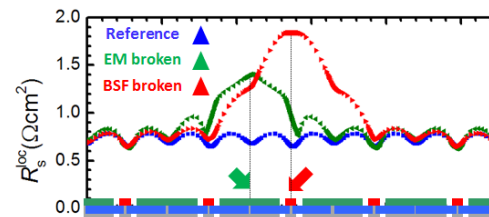


Figure 3: Simulated R_S^{loc} profiles at MPP for various scenarios of globally or locally problematic contacts

Finally, the case of locally "broken" contacts also indicates an increased R_S^{loc} for both the broken EM and the broken BSF case. However, now the targeted BSF contact shows a greater effect on R_S^{loc} . The mean R_S^{loc} of the broken EM is actually lower than that of the locally poor emitter. This alleged contradiction is a manifestation of the same effect observed in the global IV characteristic from Tab. I. Once a local contact resistance passes a design specific threshold, the high R_C impacts J_{SC} more strongly than the FF and is thus not interpreted anymore as a very high series resistance in the IV characteristic according to the diode model. This effect is thus consistent between the global analysis (double-light method for R_S^{global}) and R_S^{loc} imaging.

It is important to notice, that both in the case of the “poor” and “broken” contacts, the center of the R_S^{loc} increase was always right over the respective contact with symmetric signal intensities around the affected contact. This symmetry effect helps distinguishing whether the EM or BSF contact is the more problematic in experimental images.

As can be seen in Tab. I, R_S global is generally in very good agreement with the arithmetic mean. The arithmetic mean was chosen in accordance to [19]. For certain scenarios (e.g. 1x “broken” EM) the deviations are $> 10\%$. Such deviations however are well within the range of typical measurement errors when comparing imaging to global results in experiments [20]. However, further investigations on reasons for the deviations are necessary.

4 EXAMPLE OF A QUALITATIVE IDENTIFICATION OF CONTACT RESISTANCE PROBLEMS

The results in the previous section make clear that the IV implications of locally “poor” or “broken” contacts can be identified by experimental series resistance imaging using luminescence imaging. In this section, we comment on how luminescence image data can be used to qualitatively identify problems of contact resistance.

Fig. 4 shows photoluminescence (PL) and an electroluminescence (EL) image of a 20% efficient, $2 \times 2 \text{ cm}^2$, $1 \Omega\text{cm}$, n-type IBC cell with local R_S problems but also a global problem since the FF of 73 % was much below the cell design limit.

As explained in [18], at PL- J_{SC} (a) the carrier density distribution of non-extracted minority carriers is detected. We note that the PL signal is completely periodic over the entire structure. From PL- V_{OC} (b), we note a mostly homogenous signal with periodically increased recombination over the BSF regions (higher J_0 , lower PL) [18]. At V_{MPP} (c) however, we see increased PL in the highlighted regions I and II, which indicates that proportionally more carriers are not extracted (the marked area has been scaled differently for convenience). Since J_{SC} does not show any particular signature at I or II, this should not be a broken emitter (minority carrier collecting) finger. Also, the V_{MPP} image does not show a strong increase in signal from area II to the BSF busbar (top), therefore we do not have a case of an interrupted finger which would impact the entire area along the damaged finger. Since the V_{OC} image also does not show these effects, we attribute the effects in I and II to locally “poor” contacts. From the findings in the previous sections, we can conclude that I can be attributed to two poor emitter contacts, while in II they are caused by two adjacent poor BSF contacts. The resulting R_S^{loc} image (e) quantitatively assesses the problem. The R_S^{loc} increase in I is much larger than in II. From Quokka simulations on this cell structure (data not shown), we found that this solar cell is more sensitive to a “poor” EM than a “poor” BSF contact resistance. From this finding and including an analysis of the signal symmetry we conclude that I predominantly presents “poor” EM contacts while II presents poor BSF contacts.

Finally, the electroluminescence image in (d) at high forward bias shows a low carrier concentration around I which also hints to a locally “poor” EM contact. Around region I there is less signal and hence a lower injected

charge carrier density, which is an indicator for high contact resistance as well. In II, a distinctive contrast as at MPP conditions (c) is not observed. Since current paths in an IBC cell in the dark strongly differ from those under illumination, using electroluminescence for quantitative evaluations of local series resistance as published by Haunschild [21] is not expected to be suitable for IBC cells.

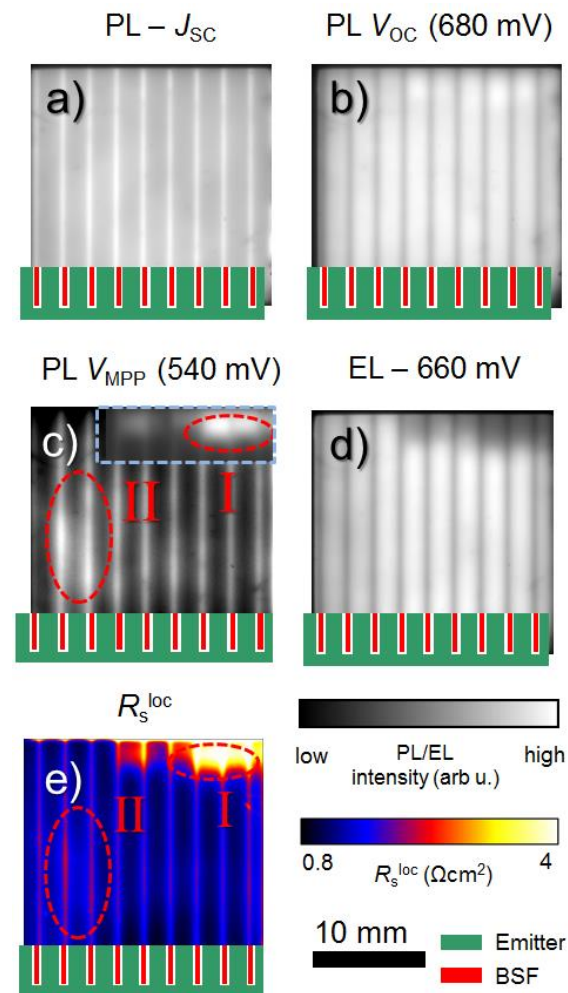


Figure 4: PL/EL and resulting R_S^{loc} images of an IBC solar cell. The J_{SC} (a) and V_{OC} (b) images have homogeneous patterns, the V_{MPP} image (c) suggests local effects of series-resistance

5 SUMMARY

In this work, we studied the impact of globally and locally deteriorated contact resistances of IBC cells on their IV characteristics and spatially resolved series resistance. We used advanced two dimensional device modeling to simulate the luminescence signature of these contact resistance problems and identify characteristic patterns in these images for emitter and BSF regions. We found that the IV characteristic and R_S^{loc} response from globally poor emitter or BSF contacts is indistinguishable. On the other hand, locally “poor” contacts have a non-identical sensitivity in FF and R_S^{loc} response. This design specific asymmetry presents important knowledge for cell manufacturers. We found that highly two dimensional and different current paths

for electrons and holes do not hinder the identification and quantification of local problems through conventional R_S^{loc} imaging and modeling of IV characteristics.

REFERENCES

- [1] F. Granek, C. Fleischmann, S. Kluska, D. Erath, and J. Rentsch, presented at the 25th EU PVSEC, Valencia, Spain, 2010 proceedings paper.
- [2] C. Reichel, Dissertation, Universität Freiburg, 2012.
- [3] B. Michl, M. Padilla, I. Geisemeyer, S. Haag, F. Schindler, M. C. Schubert, and W. Warta, accepted for publication in IEEE Journal of Photovoltaics (2014).
- [4] K. Masuko, presented at the Proceedings of the 40th IEEE Photovoltaic Specialists Conference, Denver, CO, USA, 2014 proceedings paper.
- [5] D. D. Smith, P. J. Cousins, A. Masad, S. Westerberg, M. Defensor, R. Ilaw, T. Dennis, N. Bergstrom, A. Leygo, X. Zhu, B. Meyers, B. Bourne, M. Shields, and D. Rose, presented at the Proceedings of the 39th IEEE Photovoltaic Specialists Conference, Tampa, Florida, USA, 2013 proceedings paper.
- [6] T. Trupke, E. Pink, R. A. Bardos, and M. D. Abbott, Applied Physics Letters **90** (093506), 1 (2007).
- [7] M. Padilla, B. Michl, N. Hagedorn, C. Reichel, S. Kluska, A. Fell, M. Kasemann, W. Warta, and M. Schubert, submitted for publication (2014).
- [8] R. A. Sinton, P. J. Verlinden, R. M. Swanson, R. A. Crane, K. Wickham, and J. Perkins, presented at the Proceedings of the 13th European Photovoltaic Solar Energy Conference, Nice, France, 1995 proceedings paper.
- [9] P. Saint-Cast, M. Padilla, A. Kimmerle, and C. Reichel, IEEE Journal of Photovoltaics **4** (1), 114 (2014).
- [10] S. Kluska, F. Granek, M. Rüdiger, M. Hermle, and S. W. Glunz Solar Energy Materials and Solar Cells **94** (3), 568 (2010).
- [11] A. Fell, IEEE Transactions on Electron Devices **60** (2), 733 (2013).
- [12] A. Fell, K. C. Fong, K. R. McIntosh, E. Franklin, and A. W. Blakers, Photovoltaics, IEEE Journal of **4** (4), 1040 (2014).
- [13] K. R. McIntosh, Dissertation, University of New South Wales, 2001.
- [14] M. Wolf and H. Rauschenbach, Advanced Energy Conversion **3**, 455 (1963).
- [15] M. Glatthaar, J. Giesecke, M. Kasemann, J. Haunschild, M. The, W. Warta, and S. Rein, Journal of Applied Physics **105**, 113110 (2009).
- [16] H. Kampwerth, T. Trupke, J. W. Weber, and Y. Augarten, Applied Physics Letters **93** (202102), 202102/1 (2008).
- [17] M. Hermle, F. Granek, O. Schultz-Wittmann, and S. W. Glunz, presented at the Proceedings of the 33rd IEEE Photovoltaic Specialists Conference, San Diego, USA, 2008 proceedings.
- [18] M. Padilla, H. Höffler, C. Reichel, H. Chu, J. Greulich, S. Rein, W. Warta, M. Hermle, and M. C. Schubert, Solar Energy Materials and Solar Cells **120, Part A**, 363 (2014).
- [19] B. Michl, M. Kasemann, J. Giesecke, M. Glatthaar, A. Schütt, J. Carstensen, H. Föll, S. Rein, W. Warta, and H. Nagel, presented at the Proceedings of the 23rd European Photovoltaic Solar Energy Conference, Valencia, Spain, 2008 proceedings paper.
- [20] D. Pysch, A. Mette, and S. W. Glunz, Solar Energy Materials & Solar Cells **91**, 1698 (2007).
- [21] J. Haunschild, M. Glatthaar, M. Kasemann, S. Rein, and E. R. Weber, Physica Status Solidi RRL **3**, 227 (2009).